



OPEN

Structure based virtual screening and molecular simulation study of FDA-approved drugs to inhibit human HDAC6 and VISTA as dual cancer immunotherapy

Muhammad Shahab^{1,8}, Haitham Al-Madhagi^{2,8}, Guojun Zheng¹✉, Amir Zeb³, Abdullah Fayez Alasmari⁴, Metab Alharbi⁴, Fawaz Alasmari⁴, Muhammad Qayash Khan⁵, Momin Khan⁶ & Abdul Wadood⁷✉

Cancer immunotherapy has significantly contributed to the treatment of various types of cancers mainly by targeting immune checkpoint inhibitors (ICI). Among them, V-domain immunoglobulin suppressor of T cell activation (VISTA) has been explored as a promising therapeutic target. Besides, histone deacetylase 6 (HDAC6) has been demonstrated to be efficacious target for several cancers. The current theoretical work was performed to explore the virtual repurposing of the FDA-approved drugs as inhibitors against these two (VISTA and HDAC6) cancers therapeutic targets. The crystal structure of the two proteins were downloaded from PDB and subjected to virtual screening by DrugRep webserver while using FDA-approved drugs library as ligands database. Our study revealed that Oxymorphone and Bexarotene are the top-ranked inhibitors of VISTA and HDAC6, respectively. The docking score of Bexarotene was predicted as -10 kcal/mol while the docking score of Oxymorphone was predicted as -6.2 kcal/mol. Furthermore, a total of 100 ns MD simulation revealed that the two drugs Oxymorphone and Bexarotene formed stable complexes with VISTA and HDAC6 drug targets. As compared to the standard drug the two drugs Oxymorphone and Bexarotene revealed great stability during the whole 100 ns MD simulation. The binding free energy calculation further supported the Root Mean Square Deviation (RMSD) result which stated that as compared to the ref/HDAC6 (-18.0253 ± 2.6218) the binding free energy score of the Bexarotene/HDAC6 was good (-51.9698 ± 3.1572 kcal/mol). The binding free energy score of Oxymorphone/VISTA and Ref/VISTA were calculated as -36.8323 ± 3.4565 , and -21.5611 ± 4.8581 respectively. In conclusion, the two drugs deserve further consideration as cancer treatment option.

Tumorigenesis is a multi-step successive process driven by DNA sequence mutations in the housekeeping genes leading to the transformation of cell biology succeeded by cell behavior and malignancy¹. In addition to DNA sequence mutations, heritable epigenetic changes also account for the cancer-pattern establishment. One of the epigenetic alterations implicated in almost every aspect of cancer is histone acetylation which is catalyzed by histone acetyltransferase histone deacetylase (HDAC). HDACs family constitutes many isoforms differing in location, associated genes regulation, and activity². Due to the connection between aberrant HDAC enzyme expression and various cancers, clinical trials are assessing HDAC-specific inhibitors for corresponding cancer treatments³. For instance, ACY-1215 (ricolinostat), a specific HDAC6 inhibitor, is undergoing a phase 1b trial for relapsed/

¹State Key Laboratories of Chemical Resources Engineering, Beijing University of Chemical Technology, Beijing 100029, China. ²Biochemical Technology Program, Dhamar University, Dhamar, Yemen. ³Department of Natural and Basic Science, Faculty of Science and Engineering, University of Turbat, Turbat 92600, Pakistan. ⁴Department of Pharmacology and Toxicology, College of Pharmacy, King Saud University, 11451 Riyadh, Saudi Arabia. ⁵Department of Zoology, Abdul Wali Khan University Mardan, Mardan 23200, Pakistan. ⁶Department of Chemistry, Abdul Wali Khan University Mardan, Mardan 23200, Pakistan. ⁷Department of Biochemistry, Abdul Wali Khan University Mardan, Mardan 23200, Pakistan. ⁸These authors contributed equally: Muhammad Shahab and Haitham Al-Madhagi. ✉email: zhenggj@mail.buct.edu.cn; awadood@awkum.edu.pk

refractory multiple myeloma, while ACY-241, a second-generation HDAC6 inhibitor with improved properties, is being investigated for multiple myeloma treatment. These inhibitors, along with others like A452, are part of the effort to develop targeted therapies based on the potential of HDAC inhibition in cancer treatment. Some HDAC inhibitors have already gained FDA approval, underscoring their promise in this field^{4–7}. Among them, HDAC6 is the predominant isozyme present in the cytoplasm whose primary role is to regulate tubulin⁸. HDAC6 is distinct for having two catalytic domains, CD1 and CD2, making it a valuable target for treating cancer and Alzheimer's disease^{9,10}. Additionally, HDAC6 enhances key cancer immunotherapy targets, including PD-1 and its ligand PD-L1, crucial for immune checkpoint regulation¹¹. This approach effectively addresses two goals: halting cancer progression and reversing immunosuppression, leading to enhanced leukocyte infiltration into tumor tissues¹².

VISTA (V-domain immunoglobulin suppressor of T cell activation) is a transmembrane receptor that resembles an immunoglobulin 3D structure¹³. Similarly, elevated VISTA levels are observed in late-stage oral squamous cell carcinomas, gastrointestinal and prostate cancers, contrasting with lower levels in their early stages¹⁴. It is highly expressed in hematopoietic cells in their two lineages: myeloid and lymphoid. Myeloid cells-expressing VISTA includes neutrophils and to a lesser extent monocytes and macrophages whereas naïve CD4⁺ and Foxp3⁺ regulatory T cells constitute the lymphoid lineage¹⁵. VISTA has gained wide attention as a promising therapeutic target because it poses co-stimulatory action in immune checkpoint inhibition (ICI) pathway. Indeed, majority of attention is paid not only to its ICI implication but also to its folded structure¹⁶. As a transmembrane receptor, it is composed of 3 domains: N-terminal V-domain which is very similar to PD-L1, a transmembrane domain, and a long cytoplasmic tail which resembles CD28 and CTLA-4¹⁷. The role of VISTA in immune response regulation is complex and controversial. VISTA not only acts as a ligand expressed on antigen-presenting cells (APC), but also serves as a receptor on T cells (Fig. 1). To date, most studies have described the suppressive effect of VISTA on the immune system and the ability of VISTA-deficiency or anti-VISTA treatment to upregulate immune responses¹⁸. JNJ-61610588 is a human monoclonal antibody targeting VISTA, in clinical trials for advanced cancer. It blocks VISTA signalling, enhancing T cell responses against tumors and inhibiting tumor growth. Meanwhile, a study of CA-170 (VISTA inhibitor) is still currently being conducted in advanced solid tumors or lymphomas¹⁹. The aim of this study aims to fill is the exploration of dual targeting, where both HDAC6 and VISTA are simultaneously inhibited by FDA-approved drugs. While each of these targets has been individually studied as potential therapeutic avenues, combining their inhibition could offer a synergistic effect, potentially leading to enhanced treatment outcomes. However, the exact interplay between these two targets and the potential for enhanced efficacy remain largely unexplored. By leveraging computational techniques such as, molecular docking, and MD simulation has become an increasingly important tool for drug discovery, this study offers a rapid and cost-effective way to screen a vast library of FDA-approved drugs and identify potential candidates with dual inhibitory activity against HDAC6 and VISTA. This process aids in the identification of potential candidates displaying dual inhibitory capabilities against HDAC6 and VISTA. Enhancing the scoring function, a fundamental aspect of docking, holds significance, as molecular docking methods exhibit the ability to comb through vast databases for hit identification and novel small molecule design^{20,21}. It could offer a personalized medicine approach by tailoring existing drugs for specific patients, taking into account their unique molecular profiles and therapeutic needs.

Material and methods

Overall workflow of the present study is displayed in Fig. 2.

Receptor preparation for virtual screening. In this study, two proteins i.e. HDAC6 and VISTA were targeted. The experimentally determined 3-D structures of both the target proteins (HDAC6 and VISTA) were retrieved from Protein Data Bank (<https://www.rcsb.pdb.org/>). The PDB IDs for HDAC6 and VISTA structures are 6OIL and 5EF8, respectively^{14,15}. The structures of both the target proteins were prepared by adding the polar hydrogen atoms and other missing atoms, removing co-crystallized water and heteroatoms and assigning partial

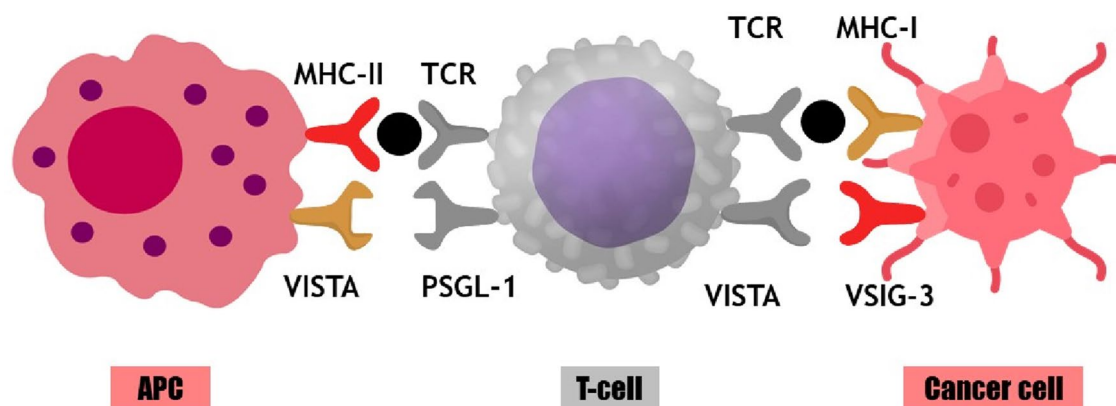


Figure 1. Interaction among antigen-presenting cell, T-cell and cancer cells by immune membrane receptors. MHC major histocompatibility complex, PSGL-1 P-selectin glycoprotein ligand-1, VSIG-3 V-Set and immunoglobulin domain containing receptor 3.

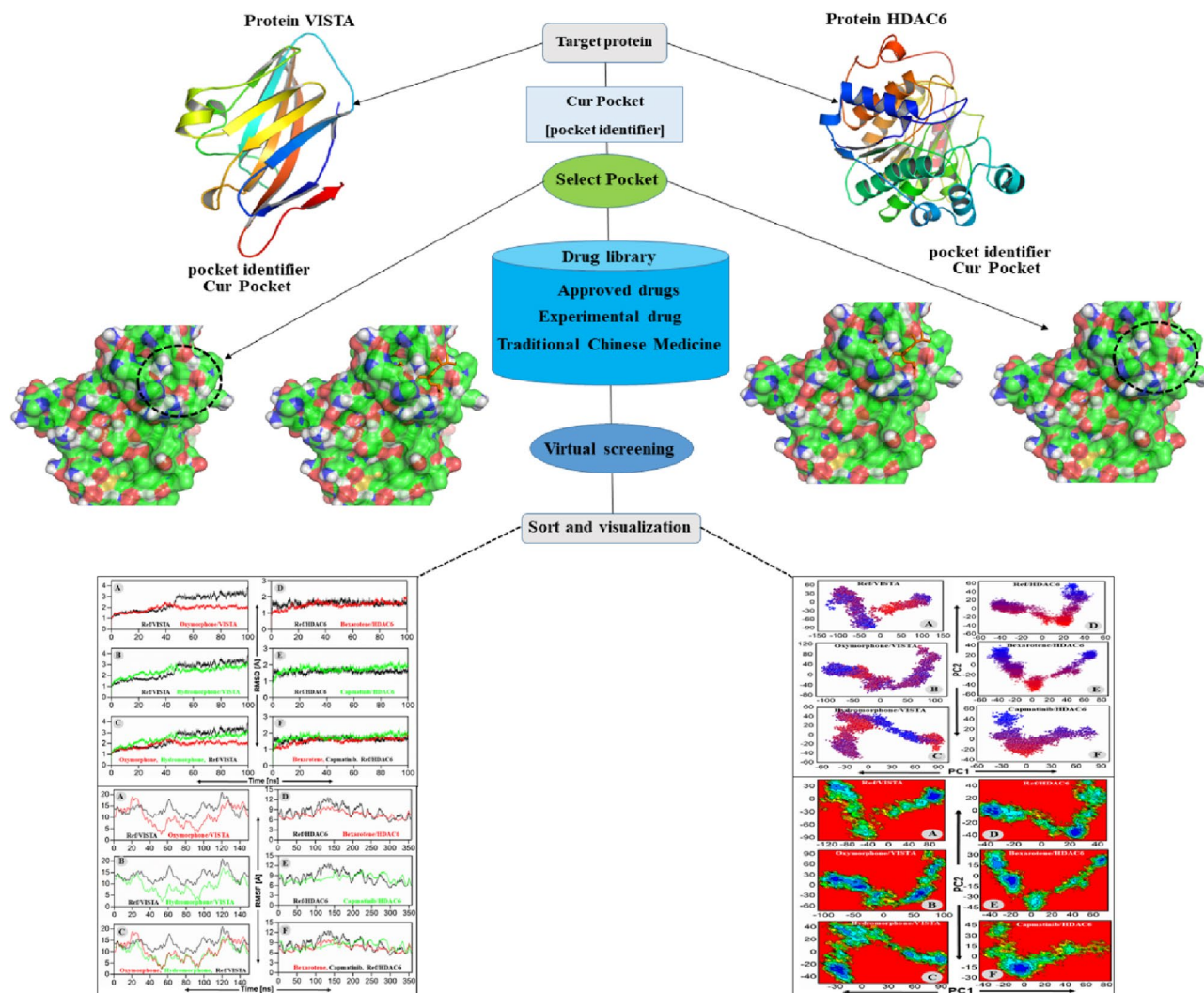


Figure 2. Step-wise workflow of the present study.

charges and their energies were minimized by employing the conjugate gradient and steepest descent algorithms of UCSF Chimera v1.16²². Since, the structure of HDAC6 is comprised of two chains, only chain A was selected during the docking operations.

Ligands library preparation for virtual screening. For ligands library preparation, the FDA-approved drugs library (2315 drugs) was selected²³. All the FDA-approved drug molecules were downloaded from Drug Bank (<https://go.drugbank.com/>) in structured data file sdf format. The structures of FDA-approved drug molecules were energy minimized and prepared as ligands library for virtual screening. This library was selected as we purposed to perform drug repurposing of FDA-approved drugs.

Virtual screening. Herein, the virtual screening was executed by the recently developed server DrugRep^{24,25}. DrugRep is a programmed and parameter-free online virtual screening server which implants AutoDock Vina algorithm for multiple ligands docking and rank the best fitted conformers of molecules by computing the docking score, binding conformation and binding affinity between the receptor and ligands structures. This server also provides pharmacodynamics services including the prediction of absorption, distribution, metabolism and excretion (ADME) properties of the top ligands²⁶. During the virtual screening by DrugRep, the previously well-prepared receptors' structures were subjected to structure-based virtual screening of the previously prepared FDA-approved drug library which contains 2315 different drug molecules (<http://cao.labshare.cn:10180/DrugRep/php/index.php>)²⁴. During the docking protocol, docking grids were generated for both the receptors including HDAC6 and VISTA. The docking grid of HDAC6 was extended enough to include almost all the binding site residues of the pocket 4 including residues Phe643, Phe642, Ser531, Gly582, Tyr745, Hsd574, Hsd614, Leu712, and Phe583. The docking grid of VISTA was architecture in such a way that it spanned the binding site residues of pocket 8 including residues Ser151 Gly130 Hsd129 Arg45 Ser8 Ala131 Val3 and Thr5.

Receptor–ligand complex analyses. To elucidate the pattern of interactions between the receptors and top-ranked drugs, Discovery Studio Visualizer 2022 was used²⁷. Both receptors in complex with their respective ligands (drug molecules) were analyzed for their interactions, binding conformation, and binding affinity (docking score). The complexes were also analyzed for their pharmacokinetics characteristics including molecular weight, number of hydrogen bond donors and acceptors and LogP values (Lipinski's rule of five)²⁸. The best fitted ligands in terms of binding affinity were selected on their best docking score, pharmacokinetics and pharmacodynamics properties.

Molecular dynamics simulation. The molecular dynamic simulation (MDS) was performed to investigate the dynamic behavior of proteins upon inhibitor binding at the atomistic level. MDS was employed to assess the stability of the compounds that had previously been recovered at the active sites of (HDAC6 and VISTA) complex. Six compounds were chosen based on their favorable interactions and docking scores. Molecular Dynamics (MD) simulations were conducted for these compounds, with three selected for each HDAC6 and VISTA protein, representing the best-fitting ligands. In case of HDAC6, the MD simulations were performed on the docked conformations of the Bexarotene, Capmatinib, and the reference compound inside the active site of the HDAC6. In case of VISTA, the MD simulations were performed on the docked conformations of the Oxymorphone, Hydromorphone and the reference compound in the active site of the VISTA protein. All simulations were performed using the ff19SB force field and the Amber22 package²⁹. During MDS, all the complexes were constructed and solved using the preparation program Tleap. Herein, a solvated octahedral box was utilized. Upon solvating each system using the TIP3P water model in an octahedral box, the complexes were neutralized by introducing counterions (Na⁺ or Cl⁻). In order to relaxing all systems, the energy of each neutralized system was minimized as much as feasible in two steps. The parameters for energy minimization included a maximum of 5000 steps using the steepest descent algorithm, followed by conjugate gradient optimization until a convergence criterion of 0.1 kcal/(mol Å) was met. The complexes after minimization were heated up to 300 K for 50 ps. Then, using a two-step process at constant pressure (1 atm) and temperature (298 K), each system was brought to equilibrium. First, a weak constraint was utilized to equilibrate the density for 50 ps. Next, we equilibrated the system for 1 ns without any restrictions. The production phase was then run for 100 ns. The pressure of each system was monitored using the Berendsen barostat, and the temperature was kept stable using the Langevin thermostat^{30,31}. We applied the AMBER22 Particle Mesh Ewald (PME) algorithm to calculate long-range electrostatic interactions. Van der Waals interactions and long-range electrostatic interactions both had a cut-off distance of 10 Å. The AMBER22 SHAKE algorithm was used to refine the covalent bonds³². All the simulations were performed using the GPU version (PMEMD.cuda) of AMBER22. The MD trajectories were examined using the AMBER22 CPPRTAJ module, PyMol v1.7, and Origin Pro Lab v2018. The interface analysis and graphical representation were completed.

Evaluation of the binding free energy. Trajectories were made with the help of MDS run while executing the MMPBSA.py script, which were then employed in the estimation of binding free energy (BFE)³³. Several studies have used this method to figure out the free energies of binding for P–P (protein–protein), protein–ligand, and nucleic acid–protein complexes²⁶. The total free energy of binding, de-noted by the symbol G_{bind}, was determined with the assistance of the following equation:

$$\Delta G_{\text{bind}} = \Delta G_{\text{complex}} - [\Delta G_{\text{receptor}} + \Delta G_{\text{ligand}}]$$

In order to gain a better understanding of how each of the energy terms, such as polar (G_{pol}), van der Waal forces (G_{vdW}), electrostatic energy (G_{ele}), no-polar interactions (G_{npol}), G_{bond} showed the angle of bond and their dihedral energy, TS represents the absolute temperature (T), and entropy (S), contribute to the total energy, the following equation was utilised (G).

$$G = G_{\text{ele}} + G_{\text{bond}} + G_{\text{vdW}} + G_{\text{npol}} + G_{\text{pol}} - TS$$

The binding free energies of the obtained complexes were calculated using the molecular mechanics generalized born surface area (MMGBSA) approach. The lower the value of the MMGBSA, which is a BFE index, the stronger the bond. The python script MMGBSA.py was used to determine the binding free energy of the obtained and standard complexes in Amber22³⁴. For complexes, the stability of the system was demonstrated by a decline in potential energy over 100 ns. After simulating for 100 ns, we look at the different shapes that emerge. In order to determine the BFE between receptor and the returned hits and the reference medicine, the MMGBSA.py script was utilized³⁵. The binding free energy (BFE) of the ligand–protein complex was evaluated using the “MMGBSA” methodology. To verify its accuracy, the results were compared and validated against the reference values for both VISTA and HDAC6. This analysis was conducted using the AMBER22 software along with the AMBER Tools MMGBSA scripts³⁶.

Results

Virtual screening. Virtual screening of FDA-approved drug library which contains 2315 different drug molecules (<http://cao.labshare.cn:10180/DrugRep/php/index.php>) was carried out by DrugRep server. According to our docking results, Bexarotene strongly bonded HDAC6 and obtained lowest docking score (–10 kcal/mol) (Table 1). The docking score of the top-10 drugs were –10 to –8.9 kcal/mol in the active site of HDAC6, which reflect their high binding energy towards the HDAC6. With respect to Lipinski's rule of five (RO5), only the best model (Bexarotene) has a single violation regarding the LogP greater than the optimal range (<5), which should not affect the pharmacokinetics characteristics of the drug since it is already FDA-approved. The

Drug name	Score	MW	HBD	HBA	RB	Rings	LogP
Bexarotene	-10	348.4779	1	2	4	3	7.6
Capmatinib	-9.5	412.428	1	5	5	5	2.9
Belinostat	-9.4	318.35	3	4	7	2	1.6
Cyproheptadine	-9.3	287.3981	0	0	0	4	4.2
Oxyphenisatin acetate	-9.2	401.418	1	3	6	4	3.4
Acrivastine	-9.2	348.4382	1	3	5	3	3.1
Ketotifen	-9.1	309.425	0	1	0	4	3.2
Phenolphthalein	-9.1	318.3228	2	3	4	4	3.8
Panobinostat	-8.9	349.434	3	2	9	3	2.9
Bisoxatin	-8.9	333.343	3	3	4	4	3.3
Reference inhibitor	-8.1	302.37	4	2	6	1	2.7

Table 1. Binding affinities as well as Lipinski's rule of five of top-10 HDAC6 inhibitors. *MW* molecular weight, *HBD* hydrogen bond donor, *HBA* hydrogen bond acceptor, *RB* rotatable bonds.

remaining drugs could strictly follow the RO5. Overall, as compared to the reference compound of HDAC6, all the top-10 drug candidates exhibited high affinity towards the HDAC6. According to our docking results, Bexarotene strongly bonded to HDAC6 and obtained lowest docking score (-10 kcal/mol) (Table 1). The docking score of the top-10 drugs were -10 to -8.9 kcal/mol in the active site of HDAC6, which reflect their high binding energy towards the HDAC6. With respect to Lipinski's rule of five (RO5), only the best model (Bexarotene) has a single violation regarding the LogP greater than the optimal range (<5), which should not affect the pharmacokinetics characteristics of the drug since it is already FDA-approved. The remaining drugs could strictly follow the RO5. Overall, as compared to the reference compound of HDAC6, all the top-10 drug candidates exhibited high affinity towards the HDAC6.

Furthermore, the binding energy of the top-10 drugs towards the VISTA receptor was significantly lower than the top-10 drugs of HDAC6 against the HDAC6 (Table 2). The energy range of the top-10 drugs was found -6.2 to -5.7 kcal/mol. It should be noted that, after docking validation, Oxymorphone binding affinity was elevated to be -7.2 kcal/mol making it the best potential VISTA inhibitor. RO5 of all top-10 drugs are within the desired range except for Zanamivir which has 11 rotatable bonds (desired < 10) (Table 2).

Receptor–ligand interaction analyses. Our study shortlisted the top-10 drug molecules that have obtained lowest docking score with HDAC6 (Table 1). The interaction analyses of the top-3 drugs suggested that drug A formed two hydrogen bonds with Asp612 and His614, drug C formed one hydrogen bond with Gly154, while the reference compound E of HDAC6 has established three hydrogen bonds with Gly154, Phe210, and His183 of the HDAC6 (Fig. 2). Apart from polar interactions (hydrogen bonds), all the three drugs also established an extensive nonpolar (hydrophobic) interactions network with several residues of the HDAC6 binding pocket (Fig. 2).

In parallel, the interaction pattern analyses of the top-2 drugs against the VISTA (Table 2) suggested that drug B formed four hydrogen bonds with Thr5 and Ala131 of VISTA, while the drug D formed three hydrogen bonds with Leu24, Arg23 and His93 of the VISTA receptor (Fig. 3). In contrast, the reference compound "F" of VISTA receptor couldn't establish a polar interaction with the binding pocket residues of VISTA during the docking operation (Fig. 3). Similarly, several nonpolar (hydrophobic) interactions between the binding site residues of the VISTA receptor and each selected drug were established (Fig. 3). The best drug candidate for HDAC6

Drug Name	Score	MW	HBD	HBA	RB	Rings	LogP
Oxymorphone	-6.2	301.3371	2	3	2	5	0.7
Hydromorphone	-6	285.3377	1	2	1	5	1.8
Morphine	-5.9	285.3377	2	2	2	5	1.5
Spectinomycin	-5.9	332.3496	5	4	5	3	-3
Zanamivir	-5.8	332.3098	7	6	11	1	-3.1
Naloxone	-5.8	327.3743	2	3	4	5	1.4
Saxagliptin	-5.7	315.41	2	3	4	5	0.7
Pirenzepine	-5.7	351.4023	1	3	3	4	0.9
Dicoumarol	-5.7	336.295	2	4	4	4	1.6
Diamorphine	-5.7	369.411	0	2	4	5	2.2
Reference inhibitor	-5.8	374.35	7	10	10	1	-6.7

Table 2. Binding affinities as well as Lipinski's rule of five of top-10 VISTA inhibitors.

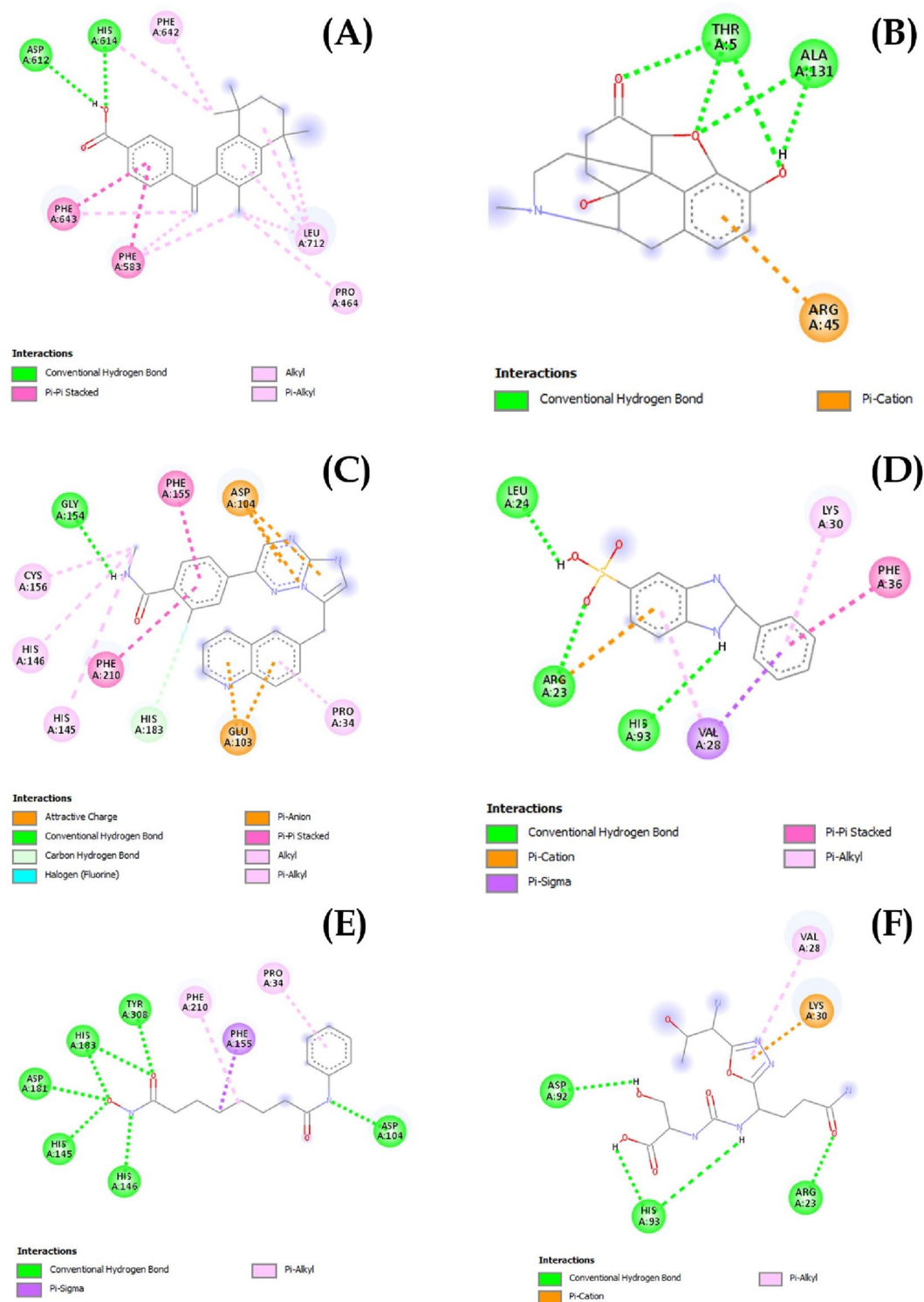


Figure 3. Receptor (HDAC6 and VISTA)-ligand interactions pattern visualized by Discovery studio. (A) and (C) refer to top 2 HDAC6 inhibitors whereas (B) and (D) refer to top 2 VISTA inhibitors. (E) and (F) refer to reference inhibitors of HDAC6 and VISTA, respectively.

(Bexarotene) was investigated for its interaction with the receptor in order to identify the catalytic residues implicated in bonding. His 573 and His 614 formed 2 H-bonds with the carboxylate oxygen atoms while Asp 612 and 705 stabilizes the interaction through forming H-bonds with the catalytic His residues. Furthermore, 3 Phe, 2 Gly along with Leu 712, Tyr 745, Ser 531 and His 574 contributed to the bonding by hydrophobic attraction as

illustrated in Fig. 2. Oxymorphone, on the other hand, was H-bonded to active site residues Thr 5 and Ala 131 while the rest of interactions was contributed by Val 3, Ser 8, His 129 and Gly 130 hydrophobic (Fig. 2).

Molecular dynamics simulation analyses. *Root means square deviation (RMSD) analyses.* The MDS results suggested two drugs named Oxymorphone and Bexarotene that could be the dual inhibitors of HDAC6 and VISTA. The result of MD simulation suggested that as compared to the reference compounds, the root means square deviation (RMSD) of VISTA in complex with Oxymorphone was converged right after 5 ns of the simulation and remained stable throughout the simulation period with an average RMSD value of 1.9 Å (Fig. 4A). The VISTA in complex with Hydromorphone also converged right after 5 ns of simulation and could remain stable during the entire simulation period with an average value of 2.5 Å with a slight deviation at the end of the simulation (Fig. 3, left panel). The superimposition of all the three simulated systems (reference, Oxymorphone and Hydromorphone in complex with VISTA) suggested that Oxymorphone behaved more stable which is followed by Hydromorphone as compared to the reference compound of the VISTA (Fig. 4C, left panel).

Afterwards, the result of MD simulation suggested that as compared to the reference compounds, the root mean square deviation (RMSD) of HDAC6 in complex with Bexarotene was converged right after the 2 ns of simulation and then retained stable throughout the simulation period with an average value of 1.15 Å (Fig. 4D). In parallel, HDAC6 in complex with Capmatinib also converged right after 2 ns of simulation and could remained stable during the entire simulation period with an average value of 2.5 Å RMSD as shown in Fig. 4. The superimposition of all the three simulated systems (reference, Bexarotene and Capmatinib in complex with HDAC6) suggested that both the drugs obtained same stability as compared to the reference compound of the HDAC6 (Fig. 4, right panel).

Root means square fluctuation analyses. Root means square fluctuation (RMSF) is an important parameter that describes the flexibility of each residues of the receptor. The RMSF analyses reflect the stability of the receptor in general and the fluctuation of the binding pocket residues in particular. The RMSF analyses of our result suggested that the reference compound of VISTA receptor showed high fluctuation (average value ~ 15 Å) as compared to the fluctuation observed for the complex of VISTA and Oxymorphone (average value ~ 8.5 Å) (Fig. 5A, left panel). In parallel, the Hydromorphone also exhibited lowest RMSF (average value ~ 8 Å) with VISTA (Fig. 5B, left panel). The comparative analyses suggested that both Oxymorphone and Hydromorphone

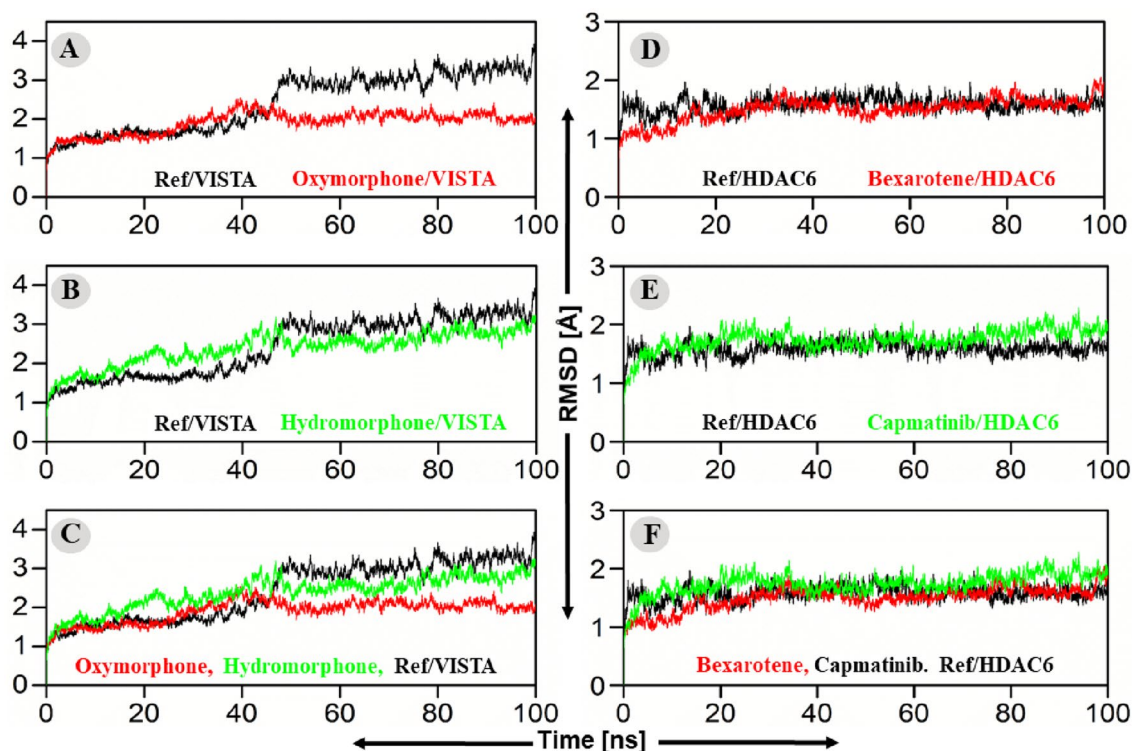


Figure 4. (A–C) RMSD Plot of the repurposed drugs/VISTA and ref-drug (CA-170)/VISTA complexes. The x-axis and y-axis showed the time in nanoseconds (100 ns) and RMSD in Angstroms respectively. (A) RMSD of Oxymorphone–VISTA complex (red) and CA-170/VISTA complex (black), (B) Hydromorphone–VISTA complex (Green) and CA-170/VISTA complex (Black) RMSD, (C) Combine RMSD compassion of VISTA. While (D–F) plot of the hits/HDAC6 and ref-drug (Trichostatin A)/HDAC6 complexes' root mean square deviations. (D) RMSD of Bexarotene–HDAC6 complex (red) and CA-Trichostatin A/HDAC6 (black), (E) RMSD of Capmatinib–HDAC6 complex (Green) and CA-Trichostatin A/HDAC6 (black), (F) Combine RMSD compassion of HDAC6.

remained more stable (average RMSF value ~ 8.2 Å) as compared to the reference compound of the VISTA protein (Fig. 5C). The RMSF analyses of HDAC6 and the candidate inhibitors suggested that the reference compound showed high fluctuation (average value ~ 8 Å) as compared to the fluctuation observed for the complex of HDAC6 and Bexarotene (average value ~ 7 Å) (Fig. 5D, right panel). In parallel, the Capmatinib also exhibited lowest RMSF (average value ~ 7 Å) with VISTA (Fig. 5E, right panel). The comparative analyses suggested that both Bexarotene and Capmatinib remained more stable (average RMSF value ~ 7 Å) as compared to the reference compound of the HDAC6 protein (Fig. 5F).

Hydrogen bonds (polar interactions) analyses. Hydrogen bond analyses is an important parameter to understand the binding affinity and stability of protein–ligand complex in drug discovery platform³⁷. Herein, the simulation results of our study showed that Oxymorphone retained a single hydrogen bond with the binding pocket residues VISTA at the middle of simulation over a period of almost 20 ns as shown in Fig. 6A, left panel. On the other hand, the Hydromorphone retained a single hydrogen bond with VISTA during the entire simulation period (Fig. 6B, left panel). The superimposed view of the hydrogen bond pattern of the reference compound, Oxymorphone and Hydromorphone with the binding pocket residues of VISTA are shown in Fig. 6C, left panel. In parallel, the simulation results of Bexarotene in complex with HDAC6 showed that Bexarotene could retain a single hydrogen bond with the binding pocket residues of HDAC6 over a short span of simulation (Fig. 6D, right panel). In contrast, the Capmatinib established and retained a single hydrogen bond with HDAC6 over the entire simulation period as shown in Fig. 6E, right panel. The superimposed view of the hydrogen bond pattern of the reference compounds, Bexarotene and Capmatinib with the binding pocket residues of HDAC6 are displayed in Fig. 6F, right panel.

Principal components analyses and free energy landscape analysis (PCA and FEL). To capture the most dominant motions during MD simulation PCA was applied to the coordinate covariance matrix derived from 100 ns MD simulation of lead compound complexes. The first two principal components (PC1 and PC2) which captures most of the motions were plotted. Here, we performed the principal VISTA and ref-drug (CA-170), Hydromorphone–VISTA complex, Oxymorphone–VISTA complex, ref-drug (Trichostatin A)/HDAC6, Bexarotene–HDAC6 complex, Trichostatin A/HDAC6, Capmatinib–HDAC6 complex, and Trichostatin A/HDAC6 complexes. The color gradient (blue to red) in the figure highlights the periodic changes in conformation.

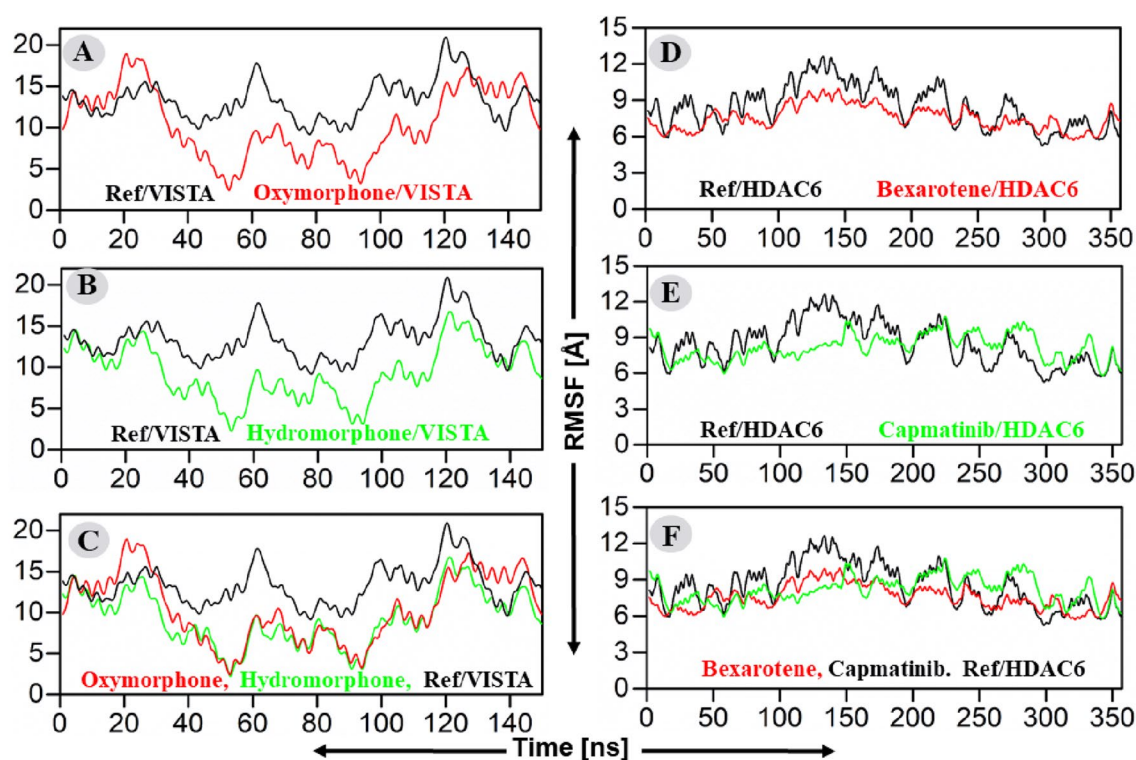


Figure 5. (A–C) RMSF plots of the repurposed drugs/VISTA and ref-drug (CA-170). The x-axis and y-axis showed the time in nanoseconds (100 ns) and RMSF in Angstroms respectively. (A) RMSF of Oxymorphone–VISTA complex (red) and CA-170/VISTA complex (black), (B) Hydromorphone–VISTA complex (Green) and CA-170/VISTA complex (Black) RMSF, (C) Combine RMSF compassion of VISTA. While (D–F) plot of the hits/HDAC6 and ref-drug (Trichostatin A)/HDAC6 complexes' root mean square deviations. (D) RMSF of Bexarotene–HDAC6 complex (red) and CA-Trichostatin A/HDAC6 (black), (E) RMSD of Capmatinib–HDAC6 complex (Green) and CA-Trichostatin A/HDAC6 (black), (F) Combine RMSD compassion of HDAC6.

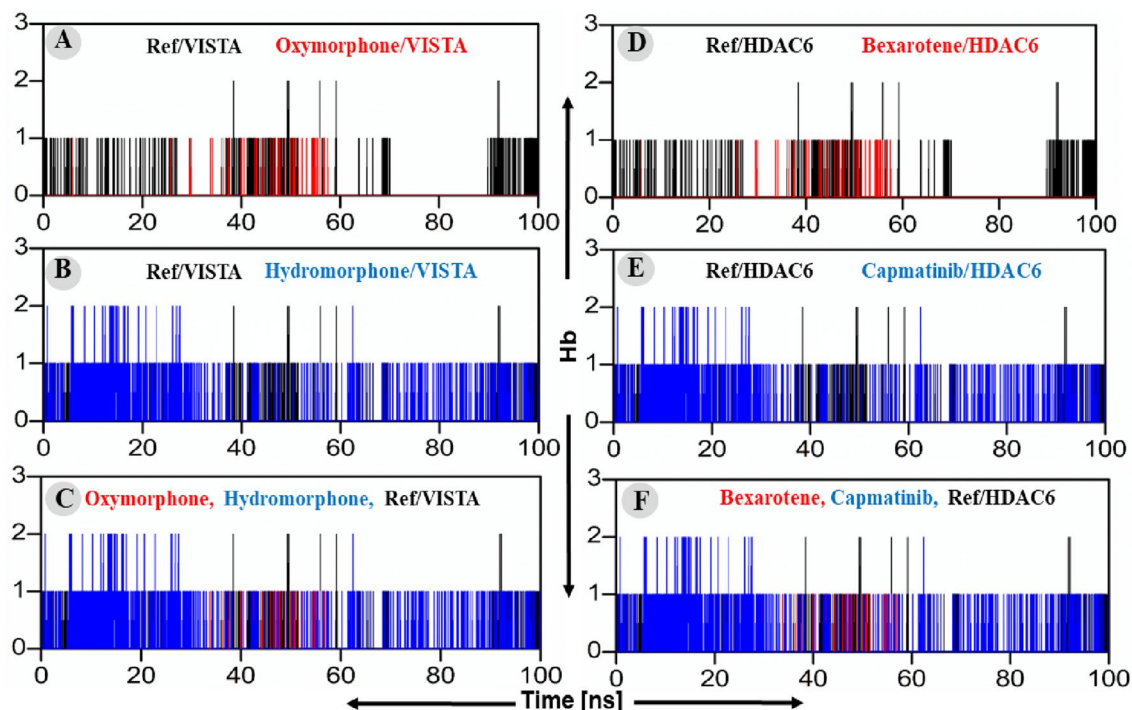


Figure 6. (A–C) Plot of the hits/VISTA and ref-drug (CA-170)/VISTA complexes' hydrogen bonding. The x-axis and y-axis showed the time in nanoseconds (100 ns) and hydrogen bonding in Angstroms respectively. (A) Hydrogen bonding of Oxymorphone–VISTA complex (red) and CA-170/VISTA complex (black), (B) Hydromorphone–VISTA complex (Blue) and CA-170/VISTA complex (Black) Hydrogen bonding, (C) Combine Hydrogen bonding comparison of VISTA. While (D–F) plot of the hits/HDAC6 and ref-drug (Bexarotene)/HDAC6 complexes' root mean square deviations. (D) Hydrogen bonding of Bexarotene–HDAC6 complex (red) and Trichostatin A/HDAC6 (black), (E) Hydrogen bonding of Capmatinib–HDAC6 complex (Blue) and Trichostatin A/HDAC6 (black), (F) Combine Hydrogen bonding comparison of HDAC6.

According to PCA each complex had different motion patterns. The ref compound's motion was slightly dispersed (Fig. 7A), with blue dots at the start, and red at the end. In contrast, compound Oxymorphone display cluster and compact type of motion compared to the ref (Fig. 7B), covering a range of -100 to $+100$ along PC1 and -80 to $+120$ along PC2. The second inhibitor Bexarotene also revealed cluster type of motion (Fig. 7C), covering a range of -60 to $+80$ at PC1 and -60 to $+340$ at PC2. The PCA analysis of all the complexes are displayed in Fig. 7. Further, the first two eigenvectors were used to calculate the free energy landscape (FEL) of VISTA and HDAC6 in complex with bound drugs. In order to comprehend the structural dynamics of each complex, the dominant and metastable state conformations were calculated from the FEL during the 100-ns MD simulation (Fig. 8). The lowest Gibbs energy states are indicated by the blue color. Different colors were used in the plot to depict high and low-energy states. Blue color indicates a low energy level, while red color indicates a high energy state. The blue color is more prevalent in ligands Oxymorphone–VISTA complex, Hydromorphone–VISTA, Bexarotene–HDAC6, and Capmatinib–HDAC6 complex, which demonstrate high stability of these drugs during MD simulation.

Binding free energy calculation. The binding free energy (ΔG_{bind}) is calculated as the difference in the solvation free energy of the complex and the solvation free energy of the individual components. The non-bonded energy ($\Delta G_{\text{non-bonded}}$) is calculated as the difference in the non-bonded interactions between the complex and the individual components. Molecular Mechanics Generalized Born Surface Area (MMGBSA), a well-known technique, has been used to accurately predict the binding free energies of all the complexes. Gibbs free energy controls the binding affinity between the interacting molecules^{38,39}. The total binding free energies of all the retrieved hits along with the reference complex as well as van der Waals, electrostatic energy, polar solvation energy and other energies terms. These finding strongly support that our retrieved hits had greater potential for inhibition than the reference compounds. The active lead in the database Bexarotene/HDAC6, had an even lower MMGBSA score of -51.9698 ± 3.1572 kcal/mol, Capmatinib/HDAC6 showed -48.8880 ± 5.7236 , and ref/HDAC6 showed -18.0253 ± 2.6218 while Oxymorphone/VISTA, Hydromorphone/VISTA, and Ref/VISTA showed the MMGBSA score -36.8323 ± 3.4565 , -25.7331 ± 1.1980 , and -21.5611 ± 4.8581 respectively. Based on these results, it can be deduced that the hits that were retrieved had good free binding energy score (average \pm standard error of the mean (SEM)) than the reference compound.

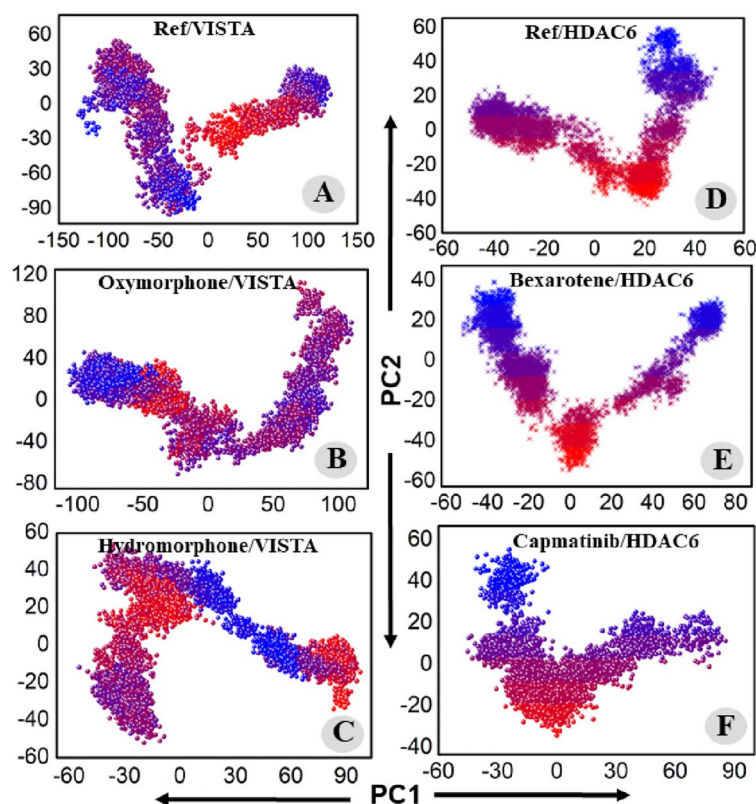


Figure 7. (A–C) PCA plots of the Ref/VISTA, Oxymorphone–VISTA, Hydromorphone–VISTA While (D,E) plot of the ref-drug/HDAC6, Bexarotene–HDAC6, and Capmatinib–HDAC6 complex.

Discussion

Cancer immunotherapy is paying much attention in the recent years with the accumulating evidences elucidating the exceptional role of immune system to defend body from cancer initiation, progression and metastasis⁴⁰. When cancer cells invade an intact tissue, the immune system if recognized such transformed cells as cancerous should eradicate cancerous cells^{41,42}. Immune system does so by reactivating the inhibited immune cells weapons to generate sufficient anti-cancer actions to eradicate the invading cancerous cells. Cancer immunotherapy empowers the braked cytokines, chemokines as well as certain immune cells to reshape the tumor microenvironment limiting the aggressive behavior of cancer⁴³. It is well known that deep epigenetic changes occur within cancer cells that aids in its progression. One of the affected enzymes are HDAC6, a novel histone deacetylase that is present in the cytoplasm hydrolyzing non-histone proteins⁴⁴. It is deemed a significant contributor to the excessive proliferation of cancerous cells and, thus, was the targets of many trials. Its inhibition displayed relative successful that benefited even standard treatment-resistant types of cancers⁴⁵. Similarly, traditional ICI like PD-L1 and CLTA-4 was also resisted by cancerous cells. On the flip side, VISTA, a negative immune regulator, is unique in its expression in naïve cells giving more opportunity of the newly formed immune cells to eradicate cancer tissue⁴⁶. Additionally, only few trials are considering VISTA as a potential ICI target⁴⁷. Therefore, the aim of this study is to screen for potential repurposable FDA-approved drugs against HDAC6 (braking the cancer progression) and VISTA (removing the imposed immunosuppression) as a novel dual therapeutic strategy for cancer treatment.

The results of the present study found that many FDA-approved drugs can replace the reference inhibitor of HDAC6 as they displayed stronger binding affinity. The ADME features of the top-10 drugs satisfy Lipinski's rule of five appropriately. The detailed enzyme-drug interaction unveiled the fit to the active site with the formation of numerous H-bonds accounting for the stronger binding affinity. The best HDAC6 potential drug was Bexarotene. Bexarotene is already in use for prevention, treatment as well as alleviating the drug-resistance of conventional chemotherapy⁴⁸. However, its use is restricted to cutaneous T-cell lymphoma and in the phase I of breast cancer clinical trial⁴⁹. On the other side, the best repurposable drug prediction to inhibit VISTA was Oxymorphone (binding affinity of -6.2 kcal/mol) with excellent pharmacokinetics profile. Oxymorphone is a typical mu-opioid agonist that is effective in both immediate- and extended-release formulations designed for pain relief⁵⁰. Therefore, coupling the blocking of cancer epigenetic regulator (HDAC6) and ICI (VISTA) with Bexarotene and Oxymorphone is an unprecedented way to aggressively limit cancer pathogenicity that deserves experimental validation.

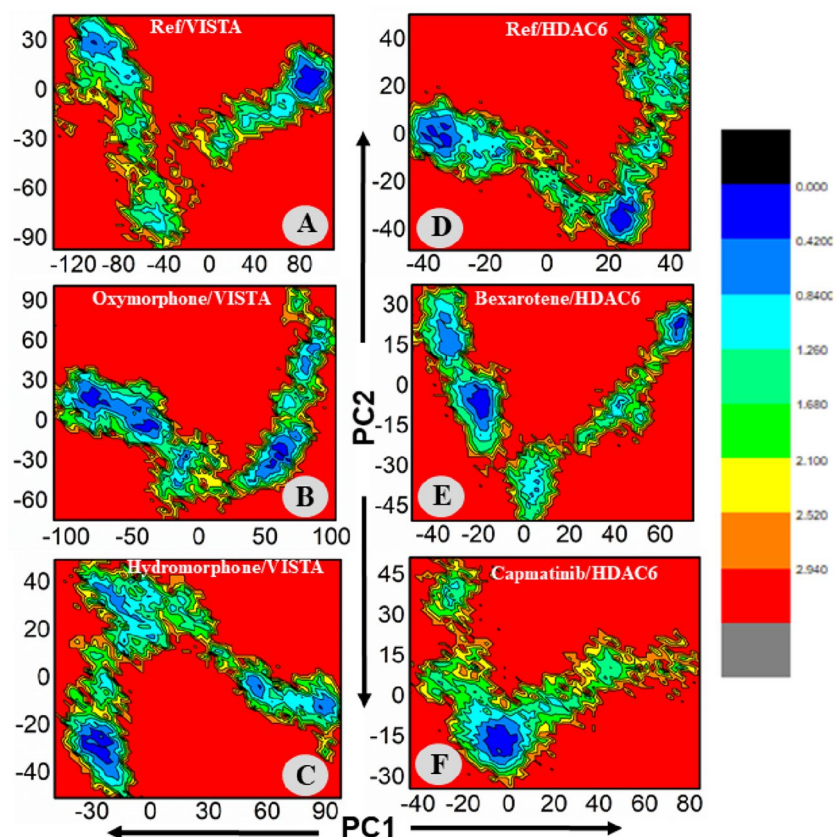


Figure 8. (A–C) FEL plots of the Ref/VISTA, Oxymorphone–VISTA, Hydromorphone–VISTA. While (D,E) plot of the ref-drug/HDAC6, Bexarotene–HDAC6, and Capmatinib–HDAC6 complex.

Conclusion

In the present study virtual screening of FDA approved drugs retrieved from the DrugBank database was carried out against the HDAC6 and VISTA cancer drug targets. Different computational tools were used in this study which leads to the identification of drugs against cancer. In terms of docking score, stability, and MMGBSA calculation the two drugs Bexarotene and Oxymorphone were found as the most effective drugs among all the drugs of the DrugBank database. Overall, the two drugs Bexarotene and Oxymorphone revealed the strong binding affinity toward the cancer drug targets HDAC6 and VISTA. These drugs can be helpful to treat cancer. However, to validate the results of our investigation, additional in vitro and in vivo studies are recommended.

Data availability

The data presented in this study are available on request from the corresponding author.

Received: 3 July 2023; Accepted: 24 August 2023

Published online: 02 September 2023

References

1. Pecorino, L. *Molecular Biology of Cancer: Mechanisms, Targets, and Therapeutics* (Oxford University Press, 2021).
2. Li, T. *et al.* Histone deacetylase 6 in cancer. *J. Hematol. Oncol.* **11**(1), 1–10 (2018).
3. Milazzo, G. *et al.* Histone deacetylases (HDACs): Evolution, specificity, role in transcriptional complexes, and pharmacological actionability. *Genes* **11**(5), 556 (2020).
4. Yoo, J. *et al.* HDAC6-selective inhibitors enhance anticancer effects of paclitaxel in ovarian cancer cells. *Oncol. Lett.* **21**(3), 1–1 (2021).
5. Yee, A. J. *et al.* Ricolinostat plus lenalidomide, and dexamethasone in relapsed or refractory multiple myeloma: A multicentre phase 1b trial. *Lancet Oncol.* **17**(11), 1569–1578 (2016).
6. Huang, P. *et al.* Selective HDAC inhibition by ACY-241 enhances the activity of paclitaxel in solid tumor models. *Oncotarget* **8**(2), 2694 (2017).
7. Lee, D. H. *et al.* The HDAC6 inhibitor ACY-1215 enhances the anticancer activity of oxaliplatin in colorectal cancer cells. *Int. J. Oncol.* **53**(2), 844–854 (2018).
8. Batchu, S. N., Brijmohan, A. S. & Advani, A. The therapeutic hope for HDAC6 inhibitors in malignancy and chronic disease. *Clin. Sci.* **130**(12), 987–1003 (2016).
9. Pulya, S. *et al.* HDAC6 as privileged target in drug discovery: A perspective. *Pharmacol. Res.* **163**, 105274 (2021).
10. Li, Y. *et al.* Inhibition of histone deacetylase 6 (HDAC6) as a therapeutic strategy for Alzheimer's disease: A review (2010–2020). *Eur. J. Med. Chem.* **226**, 113874 (2021).

11. Lucibello, G. *et al.* PD-L1 regulation revisited: Impact on immunotherapeutic strategies. *Trends Mol. Med.* **27**(9), 868–881 (2021).
12. Xu, P. *et al.* Histone deacetylase 2 knockout suppresses immune escape of triple-negative breast cancer cells via downregulating PD-L1 expression. *Cell Death Dis.* **12**(8), 779 (2021).
13. Hu, X. *et al.* M351-0056 is a novel low MW compound modulating the actions of the immune-checkpoint protein VISTA. *Br. J. Pharmacol.* **178**(6), 1445–1458 (2021).
14. Wang, B. *et al.* Overcoming acquired resistance to cancer immune checkpoint therapy: Potential strategies based on molecular mechanisms. *Cell Biosci.* **13**(1), 1–23 (2023).
15. ElTanbouly, M. A. *et al.* VISTA: A novel immunotherapy target for normalizing innate and adaptive immunity. In *Seminars in Immunology* (Elsevier, 2019).
16. Plavc, G. *et al.* Challenges in combining immunotherapy with radiotherapy in recurrent/metastatic head and neck cancer. *Cancers* **12**(11), 3197 (2020).
17. Wang, L. *et al.* VISTA, a novel mouse Ig superfamily ligand that negatively regulates T cell responses. *J. Exp. Med.* **208**(3), 577–592 (2011).
18. Martin, A. S. *et al.* VISTA expression and patient selection for immune-based anticancer therapy. *Front. Immunol.* **14**, 1086102 (2023).
19. Huang, X. *et al.* VISTA: An immune regulatory protein checking tumor and immune cells in cancer immunotherapy. *J. Hematol. Oncol.* **13**, 1–13 (2020).
20. Rasul, H. O. *et al.* Screening the possible anti-cancer constituents of *Hibiscus rosa-sinensis* flower to address mammalian target of rapamycin: An in silico molecular docking, HYDE scoring, dynamic studies, and pharmacokinetic prediction. *Mol. Divers.* <https://doi.org/10.1007/s11030-022-10556-9> (2022).
21. Meng, X.-Y. *et al.* Molecular docking: A powerful approach for structure-based drug discovery. *Curr. Comput. Aided Drug Des.* **7**(2), 146–157 (2011).
22. Pettersen, E. F. *et al.* UCSF Chimera—A visualization system for exploratory research and analysis. *J. Comput. Chem.* **25**(13), 1605–1612 (2004).
23. Wishart, D. S. *et al.* DrugBank 5.0: A major update to the DrugBank database for 2018. *Nucleic Acids Res.* **46**(D1), D1074–D1082 (2018).
24. Gan, J.-H. *et al.* DrugRep: An automatic virtual screening server for drug repurposing. *Acta Pharmacol. Sin.* **44**(4), 888–896 (2023).
25. Rasul, H. O. *et al.* Discovery of potential mTOR inhibitors from *Cichorium intybus* to find new candidate drugs targeting the pathological protein related to the breast cancer: An integrated computational approach. *Mol. Divers.* **27**(3), 1141–1162 (2023).
26. Li, A. P. Screening for human ADME/Tox drug properties in drug discovery. *Drug Discov. Today* **6**(7), 357–366 (2001).
27. Jejurikar, B. L. & Rohane, S. H. Drug designing in discovery studio. *Asian J. Res. Chem.* **14**, 135–138 (2021).
28. Chen, X. *et al.* Analysis of the physicochemical properties of acaricides based on Lipinski's rule of five. *J. Comput. Biol.* **27**(9), 1397–1406 (2020).
29. Harris, J. A. *et al.* GPU-accelerated all-atom particle-mesh Ewald continuous constant pH molecular dynamics in amber. *J. Chem. Theory Comput.* **18**(12), 7510–7527 (2022).
30. Roe, D. R. & Brooks, B. R. A protocol for preparing explicitly solvated systems for stable molecular dynamics simulations. *J. Chem. Phys.* **153**(5), 054123 (2020).
31. Aljuaid, A. *et al.* Structural homology-based drug repurposing approach for targeting NSP12 SARS-CoV-2. *Molecules* **27**(22), 7732 (2022).
32. Shahab, M. *et al.* In silico identification of lead compounds for *Pseudomonas aeruginosa* PqsA enzyme: Computational study to block biofilm formation. *Biomedicines* **11**(3), 961 (2023).
33. Junaid, M. *et al.* Structural-dynamic insights into the *H. pylori* cytotoxin-associated gene A (CagA) and its abrogation to interact with the tumor suppressor protein ASP2 using decoy peptides. *J. Biomol. Struct. Dyn.* **37**, 4035–4050 (2019).
34. Shahab, M. *et al.* Machine learning-based drug design for identification of thymidylate kinase inhibitors as a potential anti-*Mycobacterium tuberculosis*. *J. Biomol. Struct. Dyn.* <https://doi.org/10.1080/07391102.2023.2216278> (2023).
35. Khan, A. *et al.* Immunogenomics guided design of immunomodulatory multi-epitope subunit vaccine against the SARS-CoV-2 new variants, and its validation through in silico cloning and immune simulation. *Comput. Biol. Med.* **133**, 104420 (2021).
36. Shahab, M. *et al.* In silico mutagenesis-based designing of oncogenic SHP2 peptide to inhibit cancer progression. *Sci. Rep.* **13**(1), 10088 (2023).
37. Lill, M. A. & Danielson, M. L. Computer-aided drug design platform using PyMOL. *J. Comput. Aided Mol. Des.* **25**, 13–19 (2011).
38. Khan, A. *et al.* In silico mutagenesis-based remodelling of SARS-CoV-1 peptide (ATLQAIAS) to inhibit SARS-CoV-2: Structural-dynamics and free energy calculations. *Interdiscip. Sci. Comput. Life Sci.* **13**, 521–534 (2021).
39. Ghufraan, M. *et al.* In-silico design of peptide inhibitors of K-Ras target in cancer disease. *J. Biomol. Struct. Dyn.* **38**(18), 5488–5499 (2020).
40. Rasul, H. O. *et al.* In silico molecular docking and dynamic simulation of eugenol compounds against breast cancer. *J. Mol. Model.* **28**(1), 17 (2022).
41. Barrett, J. & Le Blanc, K. Cancer chemotherapy and immune regulation. *Am. J. Immunol.* **5**(1), 8–16 (2009).
42. Tan, A. C. *et al.* Systematic review of combinations of targeted or immunotherapy in advanced solid tumors. *J. Immunother. Cancer* **9**(7), e002459 (2021).
43. Sanmamed, M. F. & Chen, L. A paradigm shift in cancer immunotherapy: From enhancement to normalization. *Cell* **175**(2), 313–326 (2018).
44. Vergani, B. *et al.* Novel benzohydroxamate-based potent and selective histone deacetylase 6 (HDAC6) inhibitors bearing a pentaheterocyclic scaffold: Design, synthesis, and biological evaluation. *J. Med. Chem.* **62**(23), 10711–10739 (2019).
45. Yu, S. *et al.* Targeting HSP90-HDAC6 regulating network implicates precision treatment of breast cancer. *Int. J. Biol. Sci.* **13**(4), 505 (2017).
46. Mortezaee, K., Majidpoor, J. & Najafi, S. VISTA immune regulatory effects in bypassing cancer immunotherapy: Updated. *Life Sci.* **310**, 121083 (2022).
47. Martin, A. S. *et al.* VISTA expression and patient selection for immune-based anticancer therapy. *Front. Immunol.* **14**, 1086102 (2023).
48. Shen, D. *et al.* Emerging roles of bexarotene in the prevention, treatment and anti-drug resistance of cancers. *Expert Rev. Anticancer Ther.* **18**(5), 487–499 (2018).
49. Thomas, P. S. *et al.* Phase I dose escalation study of topical bexarotene in women at high risk for breast cancer. *Cancer Prev. Res.* **16**(1), 47–55 (2023).
50. Sloan, P. Review of oral oxymorphone in the management of pain. *Ther. Clin. Risk Manag.* **4**(4), 777–787 (2008).

Acknowledgements

Authors are thankful to researchers supporting project number (RSP2023R335), King Saud University, Riyadh, Saudi Arabia.

Author contributions

Conceptualization, A.W. and G.Z.; methodology, M.S. and H.A.M.; software, A.Z. and A.; validation, A.A. and M.A.; formal analysis, F.A. and M.Q.; investigation, M.K., A.A. and M.S.; resources, G.Z.; data curation, A., A.W. and G.Z.; writing—original draft preparation, M.S. and H.A.M.; writing—review and editing, A., A.W. and G.Z.; visualization, A.A., M.S., A.Z. and A.; supervision, A.W. and G.Z.; project administration, A.W.; funding acquisition, A.Z., M.A. and A.. All authors have read and agreed to the published version of the manuscript.

Competing interests

The authors declare no competing interests.

Additional information

Correspondence and requests for materials should be addressed to G.Z. or A.W.

Reprints and permissions information is available at www.nature.com/reprints.

Publisher's note Springer Nature remains neutral with regard to jurisdictional claims in published maps and institutional affiliations.



Open Access This article is licensed under a Creative Commons Attribution 4.0 International License, which permits use, sharing, adaptation, distribution and reproduction in any medium or format, as long as you give appropriate credit to the original author(s) and the source, provide a link to the Creative Commons licence, and indicate if changes were made. The images or other third party material in this article are included in the article's Creative Commons licence, unless indicated otherwise in a credit line to the material. If material is not included in the article's Creative Commons licence and your intended use is not permitted by statutory regulation or exceeds the permitted use, you will need to obtain permission directly from the copyright holder. To view a copy of this licence, visit <http://creativecommons.org/licenses/by/4.0/>.

© The Author(s) 2023